ADVANCED FUNCTIONAL MATERIALS
www.afm-journal.de

Cancer-Targeting Graphene Quantum Dots: Fluorescence Quantum Yields, Stability, and Cell Selectivity

Qing Zhang, Sinan Deng, Jinlin Liu, Xiaoxia Zhong, Jie He,* Xianfeng Chen,* Bowen Feng, Yanfei Chen, and Kostya (Ken) Ostrikov*

Folic acid, due to its high affinity toward folate receptors (FR), is recognized as one of the most promising cancer targeting vectors. However, the inherent defects of low water solubility (1.6 μg mL^{-1}), high sensitivity toward photobleaching, low fluorescent quantum yields (QYs, <0.5%) seriously limit its practical application. Herein, ultrastable, highly luminescent graphene quantum dots (GQDs) that selectively target diverse cancer cells are prepared and tested. The new GQDs present step changes compared to common folic acid through an ≈6250 times increase in water solubility (to ≈10 mg mL^{-1}), more than 150 times in QYs (up to ≈77%), while maintaining luminescence stability up to 98% when subjected to UV, visible light, and heating over 360 min. It is shown that the suppression of nonradiative transitions by amino groups pyrolyzed from pterin plays a key role in the mechanism of high QYs and excellent stability. The functional groups that are likely responsible for the selective targeting of cancer cells with different levels of folate receptor expression on the surface are identified. Collectively with these promising properties, the new functional graphene quantum dots may open a new avenue for cancer diagnosis, drug delivery, and therapies.

1. Introduction

Targeted and selective and cancer cell diagnostics and eradication is one of the ultimate aims of oncotherapy.[1] Differently from normal cells, specific receptors are overexpressed on cancer cell surface, to elevate nutrient uptake and ensure fast proliferation.[2] Specific molecular mechanisms of binding to the receptors help deliver fluorescent labels and therapeutic drugs, leading to targeted imaging and selective inactivation of cancer cells.[3] In addition to being cancer-specific, such probes should satisfy the stringent requirements for low biotoxicity, high stability, and strong luminescence. During the past decades, organic dyes, nanoparticles, semiconductor quantum dots, and other materials have been extensively investigated.[4] However, strong photobleaching and inferior thermal stability of conventional organic dyes, cytotoxicity of nanoparticles and semiconductor quantum dots limit their applicability.[5] It is presently extremely rare, if possible at all, to satisfy all these requirements in one single material.

Carbon quantum dots (CQDs) and graphene quantum dots (GQDs) have recently received tremendous attention because of their novel combination of tunable photoluminescence, excellent photostability, biocompatibility, and chemical inertness.[6] These unique characteristics provide unprecedented opportunities in optical bioimaging.[7] However, the fluorescent quantum yields (QYs)

Q. Zhang, Prof. X. X. Zhong, Prof X. F. Chen, B. W. Feng, Y. F. Chen
State Key Laboratory of Advanced Optical Communication Systems and Networks
Key Laboratory for Laser Plasmas (Ministry of Education)
School of Physics and Astronomy
Shanghai Jiao Tong University
Shanghai 200240, China
E-mail: xxzhong@sjtu.edu.cn; xfchen@sjtu.edu.cn

S. N. Deng
Department of Stomatology
Minghang Branch
Zhongshan Hospital
Fudan University
Shanghai 201199, China

J. L. Liu
Xiangya Stomatological Hospital
Central South University
Changsha, Hunan 410008, China

Dr. J. He
Department of Oral and Maxillofacial-Head and Neck Surgery
Ninth People's Hospital
Shanghai JiaoTong University School of Medicine
Shanghai Key Laboratory of Stomatology
and Shanghai Research Institute of Stomatology
National Clinical Research Center of Stomatology
Shanghai 200011, China
E-mail: hejie2310@126.com

Prof. K. (Ken) Ostrikov
School of Chemistry
Physics and Mechanical Engineering
Queensland University of Technology
Brisbane, QLD 4000, Australia

Prof. K. (Ken) Ostrikov
CSIRO-QUT Joint Sustainable Processes and Devices Laboratory
Lindfield, NSW 2070, Australia

The ORCID identification number(s) for the author(s) of this article can be found under https://doi.org/10.1002/adfm.201805860.

DOI: 10.1002/adfm.201805860

of CQDs and GQDs are typically quite low (<10%). Recently, it was found that nitrogen doping can significantly improve the QYs of GQDs emitting at short wavelengths (blue emission).[8] Unfortunately, their fluorescence (FL) intensity decreases sharply under UV light exposure. Furthermore, most of the GQDs are now internalized by cells in a nonspecific way. The nonselective cellular uptake limits the applicability of GQDs in cancer cells targeting therapies. It is still a challenge to prepare stable fluorescent GQDs featuring both high QYs and high-performance biological functionality.

Here, we focus on one of the most promising molecular recognition mechanisms based on the folic acid (FA) affinity of folate receptors that are overexpressed on the surface of cancer cells and are very rare (often absent) on the surfaces of normal cells.[1b,9] Due to the high binding affinity (K_d = 0.1–1 × 10^{-9} M) of FR toward FA, this means of FR targeting has been actively studied since its first discovery in 1931.[10] Recent discoveries reveal specific functions of pterin and glytamyl moieties of folic acid in targeting binding with FR for pterin and fluorescence (FL) excitation and carrying conjugated drug payload for glytamyl.[3] However, FA shows poor solubility (≈1.6 µg mL $^{-1}$ at 25 °C), strong UV degradation, and low luminescence yield (less than 0.5%).[11] When exposed to harsh conditions such as UV exposure, broken FA may lead to the loss of glytamyl-bound payload even if pterin links to FR.[12]

Here, we present an unconventional and highly promising form of a graphene quantum dot, named here folate receptor targeting graphene quantum dots (FR-GQDs). The new FR-GQDs have several clear advantages (see Tables S1 and S2, Supporting Information) compared to the existing state-of-the-art. Our custom-designed synthesis method where FA and tris(hydroxymethyl)amino methane are heated under pH-neutral conditions (see **Scheme 1**) made it possible to fully retain the selective FR targeting feature of the folic acid, and then improve the solubility in near 6250 times (from 1.6 to 10 000 µg mL^{-1}) by inserting hydroxyl functional group. The luminescence QYs increased in more than 150 times (from 0.5 to 77%) by suppressing nonradiative transitions with the newly emerged plentiful amino groups. Importantly, the new produced FR-GQDs feature highly photostable (subjected to 90.81 mW cm^{-2} photoflux for 360 min) and thermally stable (subjected to 0–95 °C temperature variation and heating at 70, 80, and 90 °C for 360 min).

Moreover, the new FR-GQDs show excellent nontoxicity (Table S3, Supporting Information), while the level of luminescence increases proportionately to the density of FR on the surface of the cells, from near zero in normal bone marrow stem cells (BMSC) to SKOV3 ovarian cancer cells where the FR are significantly overexpressed. These findings make it possible to specify the cancer states through the level of FR expression and target the cells with specific drugs. Collectively with excellent optical properties and inherent stability, the new FR-GQDs are promising for cancer targeted photodynamic and photothermal therapies, as well as super-resolution imaging, leading to potentially radically new cancer diagnostics and treatments.

Our studies further reveal the mechanism of high fluorescence QYs, photostability, and cancer targeting functionality of FR-GQDs. By comparing with the achievements of previous reports and vibration spectra between FA and FR-GQDs, we find that the amino groups derived from pterin significantly suppress the nonradiative transition of the excited FR-GQDs and subsequently enhance the FL QYs. The inherent stability of graphene nucleus, surface molecular structure, and relative low reactive oxygen species (ROS) productivity of FR-GQDs lead to stability under high flux light exposure. Furthermore, analyses of cell experiments and vibration spectra demonstrate that new functional moieties, other than pterin, are responsible for the cancer targeting functionality while still retaining FR targeting functionality. Our results suggest that when the pterin moiety of the folic acid is (at least partially) destroyed by the appropriate thermal process, the FR targeting ability is retained, while a much better QY and stability are presented. Our results may thus open generic pathways for performance improvement of pterin derivatives in a broader range of applications.

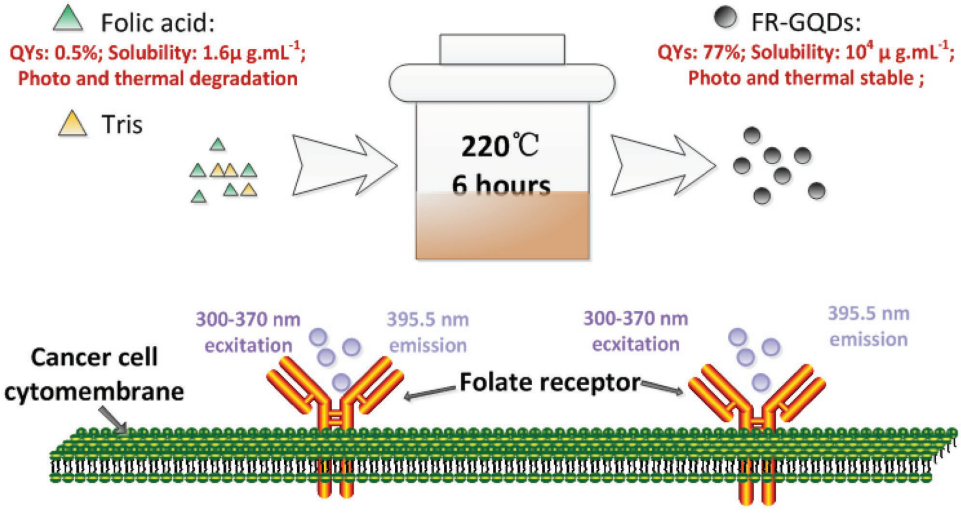

Scheme 1. Preparation, characteristics, and folate receptor binding of FR-GQDs.

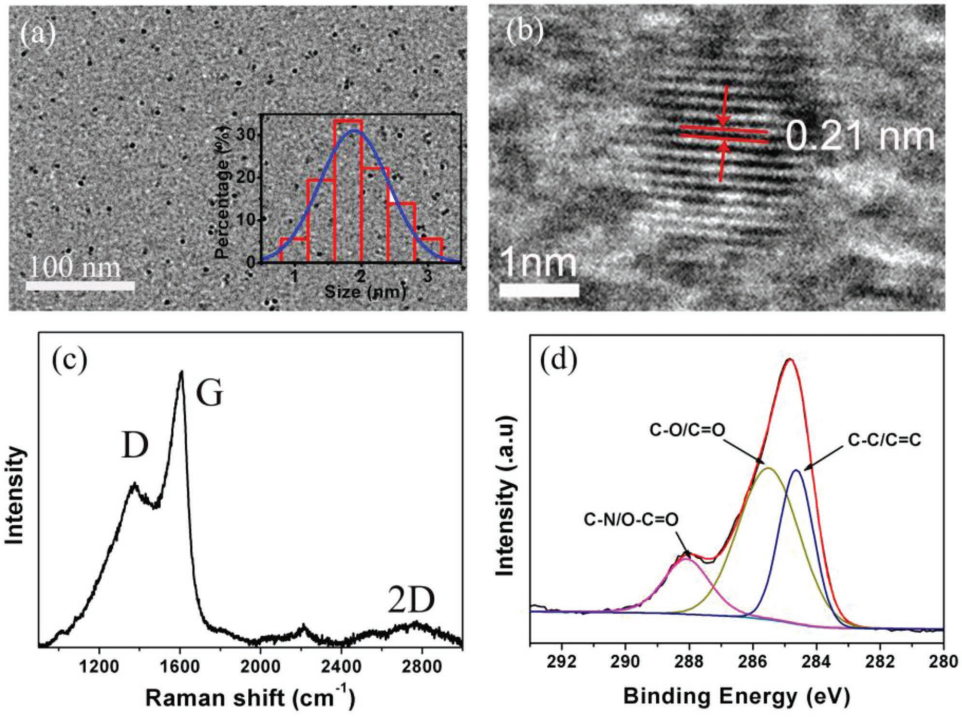

Figure 1. a) TEM images of FR-GQDs (inset: size distribution of FR-GQDs), b) high-resolution TEM images, c) Raman spectrum of FR-GQDs, and d) high-resolution C 1s spectrum of FR-GQDs. Scale bar is depicted in white. Full scale XPS spectra, high-resolution N 1s and O 1s spectrum of FR-GQDs are shown in Figure S1 (Supporting Information).

2. Results

2.1. Structure and Composition of FR-GQDs

Transmission electron microscope (TEM) images and corresponding particle size distribution (PSD) of the produced FR-GQDs are shown in **Figure 1**a. The GQDs disperse well in water solution. Inset picture of size distribution shows the FR-GQDs have PSD peak around 1.95 nm and are relatively size uniform. High-resolution images, shown in Figure 1b, demonstrate the lattice distance in the GQDs is 0.21 nm, which belongs to the (1,0,0) plane of graphite. Raman spectrum shown in Figure 1c features two peaks at 1407 and 1597 cm^{-1}, attributed to sp^3 (D) and sp^2 (G) structure of FR-GQDs, respectively. Based on the dominated strength of G peak, it can be concluded that the as-prepared GQDs have predominantly graphitic structure. X-ray photoelectron spectroscopy (XPS) measurements were performed to identify the chemical composition of the FR-GQDs. Full-scale spectrum in Figure S1a (Supporting Information) confirms the existence of carbon (70.79%), nitrogen (10.2%), and oxygen (18.71%). High-resolution spectrum of C 1s in Figure 1d revealed the presence of C−C/C=C (284.6 eV), C−O/C=O (285.4 eV), and C−N/O−C=O (288.0 eV).[13] High-resolution spectrum of N 1s shown in Figure S1b (Supporting Information) reveals the presence of two nitrogen species of pyridinic N (398.8 eV) and pyrrolic N (399.5 eV) form.[14] High-resolution O 1s spectrum shown in Figure S1c (Supporting Information) further confirms the existence of C=O (531.3 eV), C−OH/C−O−C (532.6 eV), and O−C=O (535.5 eV).[14a,15]

2.2. High Luminescence Efficiency

UV–vis absorption spectrum of FR-GQDs is shown in **Figure 2**a. It can be observed that FR-GQDs feature two absorption bands in which the band at 280 nm resulted from $\pi \rightarrow \pi^*$ transition and the other band at 320 nm is assigned to $n \rightarrow \pi^*$ transition. FL spectrum of FR-GQDs is investigated and depicted in Figure 2b. FL emission of FR-GQDs is located at the wavelength of 395.5 nm exhibiting an excitation independent behavior at excitation wavelength ranging from 300 to 370 nm. The QYs of FR-GQDs are measured using slope method in comparison with that of quinine sulfate (54%). According to the calculation results shown in Figure 2c, QYs of FR-GQDs have reached up to 77%.

2.3. Photostability and Thermal Stability

Photostability of FR-GQDs was tested by subjecting the samples to continuous 90.81 mW cm^{-2} mercury lamp exposure for 360 min. As shown in Figure S2 and Table S4 (Supporting Information), the spectra of exposure light include both of ultraviolet light (365 nm, 26.9 $mWcm^{-2}$) and visible light (404–708 nm, 63.91 $mWcm^{-2}$). Figure 2d and Table S5 (Supporting Information) show the FL intensity of FR-GQDs remained at up to 91.6% of the initial value after 360 min photobleaching. Thermal stability of FR-GQDs is investigated through two-step heating tests. They are first heated in a varied temperature range from 0 to 95 °C, and subsequently fixed at a certain temperature (70, 80, and 90 °C) for 360 min to further observe the stability. The data are shown in Figure 2e,f, Figure S4 and Tables S6 and S7

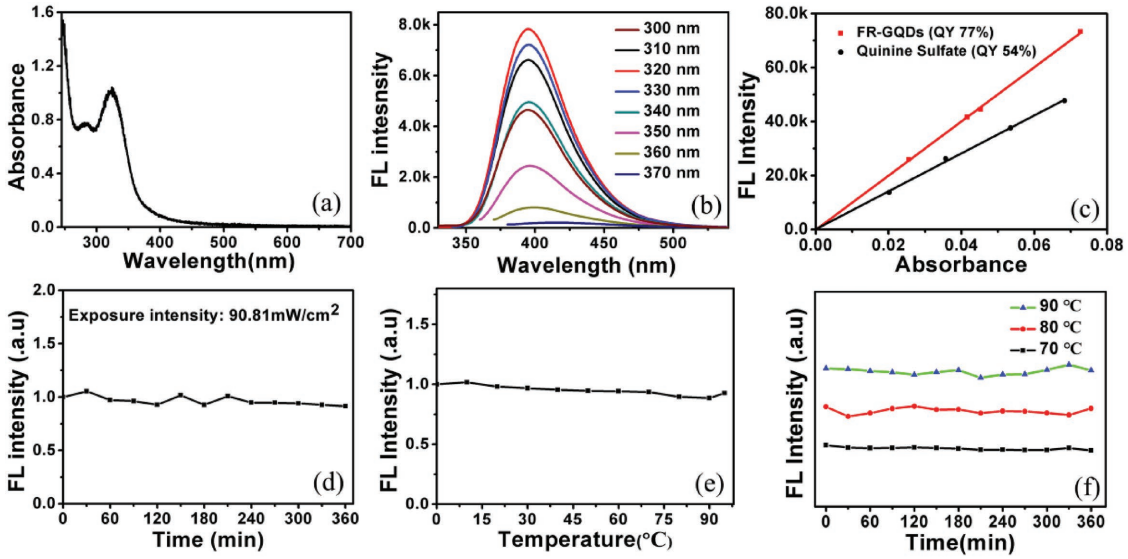

Figure 2. Vibration spectra and FL stability of FR-GQDs. a) UV–vis spectra of FR-GQDs. b) FL spectra of FR-GQDs. c) Measurement of FL QYs of FR-GQDs comparing with that of quinine sulfate. d) FL intensity of FR-GQDs samples retained up to 91.6% after subjecting to UV mercury lamp (90.81 mW cm^{-2}) illumination for 360 min. e) FL intensity of FR-GQDs samples remains stable at temperatures ranging from 0 to 95 °C and preserved 92.7% at 95 °C. f) FL intensity of FR-GQDs remains stable when the temperature is fixed at 70, 80, and 90 °C for 360 min.

(Supporting Information). As the temperature increased, fluorescence intensity of FR-GQDs decreased smoothly and stabilized at 92.7% at 95 °C. When the temperature was fixed at 70, 80, and 90 °C, the FL intensity of FR-GQDs is also highly stable (retained up to 98%) to the continuous thermal treatment.

2.4. Functionality: Cancer-Specific Targeting through FR Associating Cellular Uptake

2.4.1. Selective Binding to Cells with Different FR Expression

To test the selective FR targeting ability of FR-GQDs, cancer cells with varied FR expression including SKOV3, MDA-MB-231 (FR overexpression), MCF7 (FR middle expression), and normal bone marrow stem cell (BMSC, FR deficient) are first treated with FR-GQDs and imaged using fluorescence microscope.[16] **Figure 3**a–d are the images of BMSC, MCF7, MDA-MB-231, and SKOV3 in bright field. Figure 3e–h are the FL images of these cell samples under UV excitation. It can be observed, in Figure 3e–h, cancer cells of SKOV3, MDA-MB-231, and MCF7 with folate receptors all exhibit intense blue FL emission under UV irradiation. Nevertheless, in the case of normal cell with no FR expression, no FL signal is observed. Furthermore, the merged images depicted in Figure 3i–l show that the FL emission of FR-GQDs perfectly matches with cancer cells. These evidences confirm that the as-prepared FR-GQDs can selectively label cancer cells with different levels of FR expression.

2.4.2. Selective Uptake: FR Expression-Specific Cellular Internalization

To further verify the selectivity of FR-GQDs between cancer cells, cell samples treated with FR-GQDs are measured using fluorescent quantitative analyses. As shown in Figure 3m, in accordance with the results of FL imaging, ovarian cancer cell SKOV3 and breast cancer MDA-MB-231 display the most pronounced FL intensity, agreeing with its abundant FR distribution. The FL intensity of MCF7 cancer cell is in a medium level which is much lower than that of SKOV3 and MDA-MB-231, while remarkably stronger than the BMSC. The FL of BMSC is very weak, can even be ignored. Since the degree of FR expression follows the sequence that SKOV3 > MDA-MB-231 > MCF7 > BMSC. As such, the variation of FL intensity of comparative analyses is clearly in accordance with the evolution of FR expression on the cell surface indicating that the as-prepared FR-GQDs may be internalized by cancer cell through the cellular uptake associating with FR.

2.4.3. GQD Uptake Suppression: Competitive Effect of FA

To further explore the internalization mechanism of FR-GQDs, a competitive advantage experiment is performed. Cells of SKOV3 are first pretreated with free folic acid at concentrations ranging from 0 to 1000 μg mL^{-1} before the treatment of FR-GQDs. After being treated with FR-GQDs for 4 h and washed for three times with phosphate buffered saline (PBS), the FL intensity of FR-GQDs inside the cells is recorded using the automatic microplate reader and compared with the cell groups without FA pretreatment. As presented in Figure 3n, the inhibiting effect of FA is emerged at the concentration of 50 μg mL^{-1} with a decrement of 25% in FL intensity of FR-GQDs. When the concentration of FA reached up to 100 μg mL^{-1}, FL intensity of FR-GQDs reduces more than 70%. With the increasing concentration of FA, FL intensity of FR-GQDs finally reduced more than 85% in this study. Thus, the uptake of FR-GQDs is effectively suppressed with free folic acid. Since FA is directly

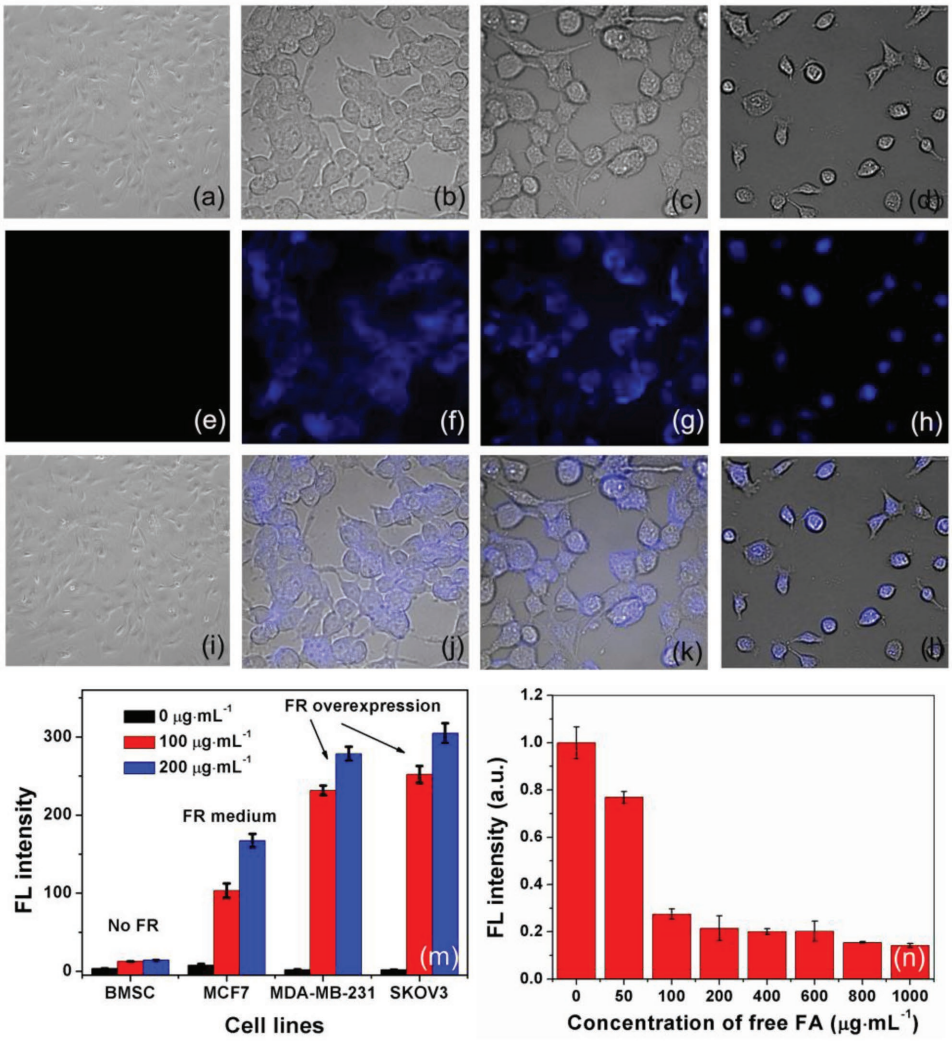

Figure 3. a–d) Cell images of BMSC, MCF7, MDA-MB-231, and SKOV3 under bright field; e–h) FL image of these samples under excitation of UV irradiation; i–l) merged cell images of bright field and UV excitation. m) FL quantitative analysis of FR-GQDs internalized in cell lines of BMSC, MCF7, MDA-MB-231, and SKOV3. FL intensity of cell samples shows direct correlation with the evolution of the FR expression on cancer cell surface. n) Evolution of FL intensity of FR-GQDs internalized in SKOV3 cells pretreated with varied concentrations of free folic acid. Cellular uptake of FR-GQDs is significantly inhibited in the presence of FA which indicates that the FR-GQDs follow a FR associating cellular uptake mechanism. (BMSC, FR deficient; MCF7, FR medium expression; MDA-MB-231 and SKOV3, FR overexpression).

internalized into cell through FR binding, the inhibitory effect of FA on the cellular uptake of FR-GQDs in this study indicates that the FR-GQDs are also internalized into cells through the FR associating cellular uptake mechanism, which is in accordance with previous reports.[16b,17]

Collectively, the results of Section 2.4.1 (fluorescence imaging), Section 2.4.2 (fluorescent quantitative analysis), and Section 2.4.3 (GQD intake suppression by a competitive mechanism) suggest that the produced FR-GQDs target cancer cells through the cellular uptake mechanism associating with FR.

2.5. Intracellular Trafficking and Cellular Distribution

Intracellular trafficking, internalization, and distribution of FR-GQDs within the cells are important for practical applications. To study these phenomena, the SKOV3 cancer cells with high FR expression are treated with FR-GQDs for 1, 2, 3, 6, and 18 h and imaged using confocal microscopy (Leica SP8, Germany) at high resolution. The results are shown in **Figure 4**. For better contrast, transmission images are set in green, while the FL signal of FR-GQDs is presented in yellow. In the first 2 h (Figure 4a,b), the FR-GQDs are seen to mostly distribute around the cytoplasm. The increasing FL signal of FR-GQDs within the cells (shown in Figure 4b) indicates that more GQDs are internalized with longer incubation time. After 3 h, the image in Figure 4c shows the FR-GQDs gradually accumulate on specific organelles of cells. These FL islands may be attributed to the multivesicular bodies (MVBs) of the endosome around the cell nucleus. After 6 and 18 h incubation, the FL intensity of GQDs (shown in Figure 4d,e) is enhanced, while even more FR-GQDs are found in the MVBs. These results are

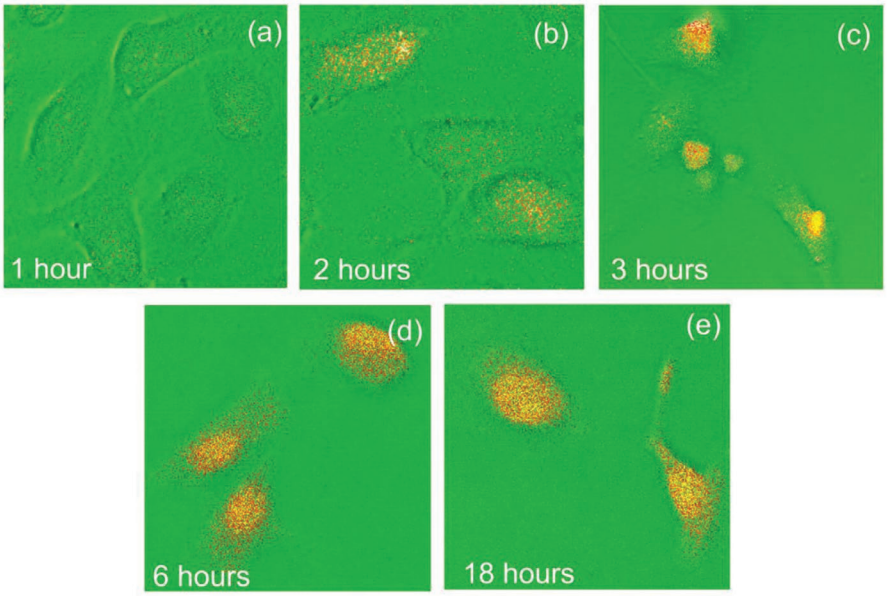

Figure 4. Confocal images showing the cellular trafficking and internalization of FR-GQDs in SKOV3 cells (high FR expression). Green channel shows the transmission images, while the yellow channel shows the fluorescence signal. The results demonstrate that the FR-GQDs prepared in our work feature quite similar cellular trafficking mechanism and cellular distribution character compared to folic acid.

in accordance with the previous studies where quantum dots were conjugated with folic acid and then internalized by the cells through the FR binding and endocytosis.[17] Therefore, it can be concluded that the FR-GQDs prepared in our work are primarily distributed around the cell nucleus, and exhibit quite similar features of intracellular trafficking and distribution as in the previous report where folic acid was used.

2.6. Biocompatibility, Nontoxicity in Vitro

To assess the cytotoxicity of FR-GQDs, cell lines of BMSC, HN-6, Cal-27, MCF7, MDA-MB-231, and SKOV3 are incubated with FR-GQDs samples at concentrations of 200, 400, 600, 800, and 1000 μg mL^{-1} for 24 h. Then a CCK-8 viability assay is carried out. The results are shown in **Figure 5** and Table S3 (Supporting Information). In comparison with the cells untreated with FR-GDQs, the viability of cancer cell groups of SKOV3, MDA-MB-231, Cal-27, and HN-6 is higher than 94% up to concentration of 1000 μg mL^{-1}. Cell groups of MCF7 are slightly more sensitive to the concentration of FR-GQDs. It shows decrease in cell viability from 94.6 to 85.7%. Viability of normal BMSC cells improves during the FR-GQDs treatment. When the drug concentration increased from 200 to 1000 μg mL^{-1}, cell viability of normal BMSC shows an increase from 105.9 to 119.4%. These data demonstrate that the produced FR-GQDs are nontoxic to cells.

3. Discussion

3.1. Characteristic Vibration Spectra

To understand the mechanisms of the high fluorescence quantum yield, photostability, and folate receptor targeting ability of the produced FR-GQDs, characteristic vibration spectrum (UV–vis, FL, Fourier transform infrared (FTIR), and ^{13}C NMR) of the FR-GQDs and FA are both recorded and compared in detail. UV–vis absorption spectra of FR-GQDs and FA are shown in **Figure 6**a. FA features two absorption bands in which the absorption band at 280 nm resulted from $\pi \rightarrow \pi^*$ transition of *para*-aminobenzoic acid and the absorption band at 365 nm is assigned to $n \rightarrow \pi^*$ transition of pertrin.[18] In the case of FR-GQDs, in comparing with the UV–vis spectra of FA, absorbance at 280 nm is significantly decreased. Absorption band of pterin of FA at 365 nm disappeared, new absorption band at 330 nm emerged. Absorption edge of FA blueshifts from 411 to 364 nm (see inset of Figure 6a) after thermal process.

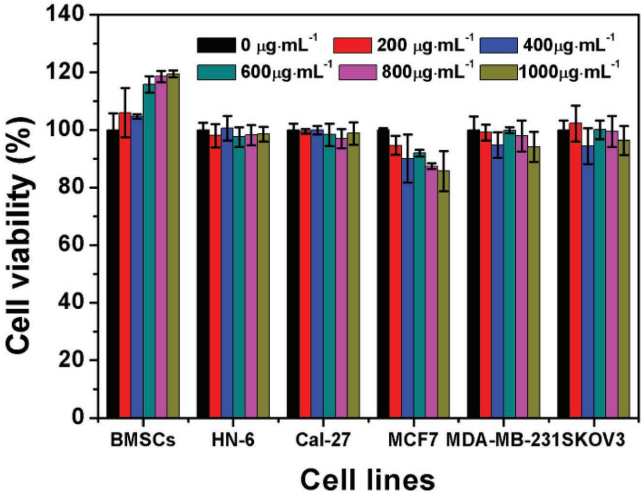

Figure 5. Cell viability of BMSC, NH-6, Cal-27, MCF7, MDA-MB-231, and SKOV3 cell lines treated with FR-GQDs samples for 24 h. No toxicity is observed, except for MCF7 cell lines (decreased to 85.7%).

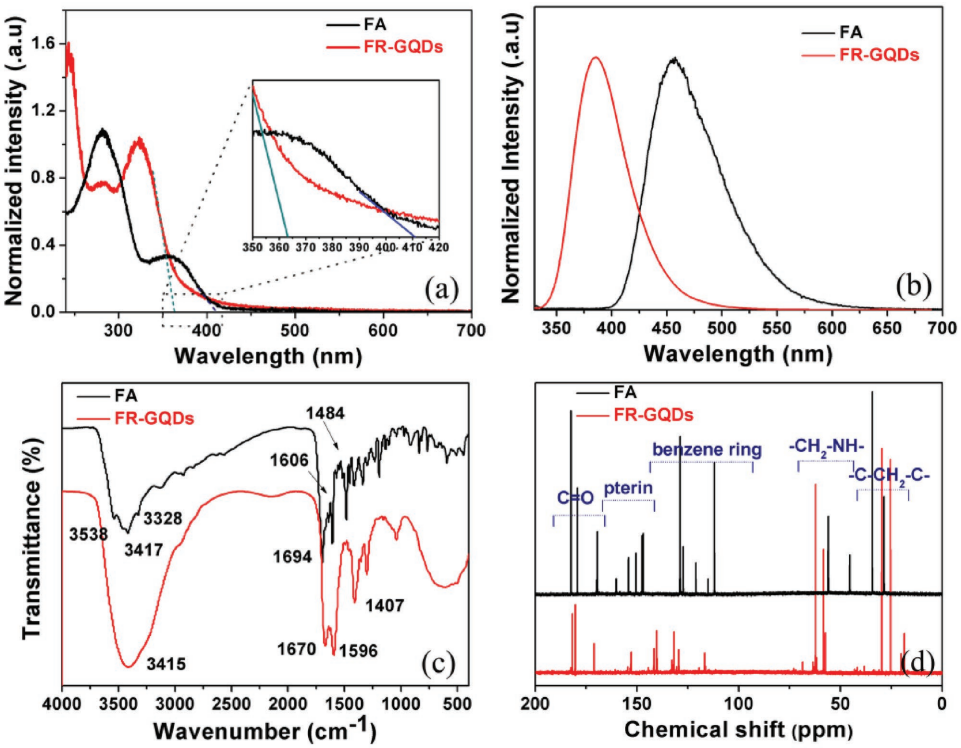

Figure 6. Characteristic vibration spectra of FR-GQDs in comparison with that of folic acid (FA). a) UV–vis spectra, b) fluorescence spectra, c) FTIR spectra, and d) ^{13}C NMR spectra of FA and FR-GQDs. During the thermal process, pterin aromatic nucleus of folic acid responsible for FR targeting is destroyed and converted to new groups featuring $-C-CH_2-C-$ and $-CH_2-NH-$ (or NH_2) structures on FR-GQDs.

Fluorescence spectra of FA and FR-GQDs are also recorded and shown in Figure 6b. It can be observed that the emission peak of pterin of FA is located at 445 nm, while the fluorescence peak of FR-GQDs is shifted to 395.5 nm.[18]A blueshift of 61.5 nm in wavelength is obtained.

FTIR spectra are presented in Figure 6c. The absorption of FA at 3417 cm^{-1} is due to hydroxy (OH) stretching vibration. Absorption peaks at 3538 and 3328 cm^{-1} correspond to stretching vibration of amino groups. Peaks at 1694 cm^{-1} are attributed to the vibration of carbonyl (C=O) from carboxylic acid group. Peaks at 1606 cm^{-1} are caused by the bending mode of amino group vibration. Stretching vibrations of pterin (C_3N_3) and benzene rings are confirmed by absorption peaks around 1484 cm^{-1}.[19] In the spectra of FR-GQDs, new absorption peaks at 1670 and 1596 cm^{-1} emerged ascribed to C=O and NH_2 stretching modes, respectively.[20] The relative strength of NH_2 stretching is significantly increased. Pterin peaks of FA around 1484 cm^{-1} disappeared after thermal processing.

^{13}C NMR results are shown in Figure 6d. In the ^{13}C NMR spectrum of FA, chemical shift at ranges of 28.4–34.3 and 45.3–60.5 ppm is attributed to the methylene carbons vibration of $-C-CH_2-C-$ and $-CH_2-NH-$ groups, respectively. Peaks between 111.8 and 150.4 ppm are due to the carbon vibration of benzene ring. The peaks from 128 to 179 ppm represent carbons of pterin ring. Peaks at 169.3, 179.4, and 182.3 ppm belong to the carbons of $-CO-NH-$ and carboxyl groups ($-COOH$), respectively. After thermal processing, chemical shifts of FR-GQDs for methylene carbons at 25.3, 29.6, 57.4, 58.3, and 62.1 ppm are significantly increased. Meanwhile, the chemical shifts of benzene ring and pterin ring ranging from 110 to 170 ppm decrease or disappear. In detail, characteristic chemical shift of pterin located at 128.8, 147.0, 147.3, 154.1, 160.1, and 179.2 ppm disappears.[21] Residual C—N, N—C=O, and N—C—N structures of pterin are thus retained and show characteristic vibrations at 129.4, 152.8, and 180.0 ppm. We can thus surmise that during the thermal process, the pterin aromatic nucleus of the folic acid is (at least partially) destroyed. Meanwhile, the new $-C-CH_2-C-$, $-CH_2-NH-$, or NH_2 groups emerge on FR-GQDs while other groups still remain and are distributed on the FR-GQDs surface. Due to the critical roles of pterin in UV–vis absorption and FL emission of FA,[18] it can be concluded that the changes in structure led to the increment of the bandgap between the lowest unoccupied molecular orbital (LUMO) and the highest occupied molecular orbital (HOMO) levels which eventually caused the blueshift of the absorption spectrum and FL emitting spectrum.

3.2. Mechanism of High Fluorescence Quantum Yields

At present, actual mechanism of the fluorescence of graphene quantum dots is still a debate among researchers.[22] A dominant perception is that surface state and quantum confinement effects of conjugated π-domains in GQDs are critical in determining the optical properties. For example, chemical groups of both $-CONHR$ and $-CNHR$ can effectively suppress the nonradiative process, then further enhance the intrinsic fluorescence emission of GQDs (QYs 59.2%).[23] Further, the synergy

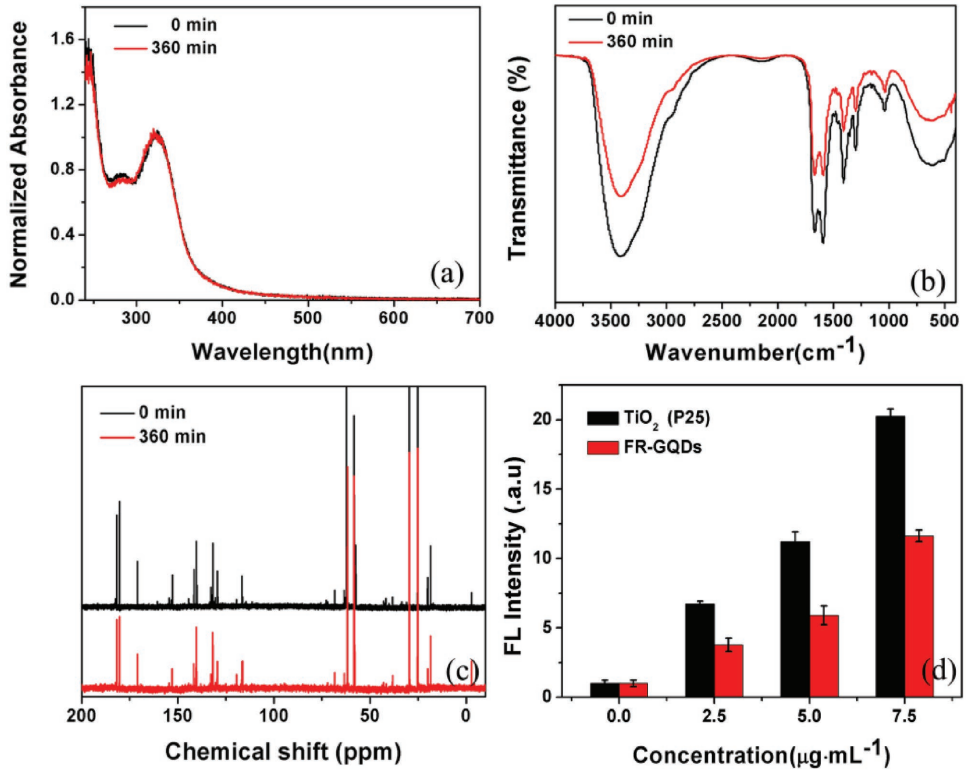

Figure 7. Vibration spectra of a) UV–vis, b) FTIR, and c) ^{13}C NMR of FR-GQDs samples at the beginning and after 360 min of light exposure (including UV light 26.8 mW cm^{-2} and visible light 64.01 mW cm^{-2}). d) Reactive oxygen (ROS) production of FR-GQDs under UV excitation (1.475 mW cm^{-2}, 10 min) at varied concentration and ROS production of titanium dioxide (TiO_2 (P25), Degussa, Germany). Vibration peaks of the two intervals match perfectly indicating the graphene nucleus and surface molecular structure of FR-GQDs remain excellent stable during photobleaching. The ROS production of FR-GQDs is about 52–56% of the TiO_2, which indicates that the ROS concentration is at the relative low level during photobleaching. Thus, it can be concluded that inherent stability of graphene nucleus, surface molecular structure of FR-GQDs, and relative low ROS productivity lead to high stability against photobleaching. (FL intensity of ROS probe is normalized by comparing with the groups of deionized water.)

effect of graphitic nitrogen and hydroxyl can significantly optimize the ratio of the radiative transition rate and eventually lead to ultrahigh QYs (99%) of GQDs.[24] In our case, results of XPS show that the content of nitrogen doped in FR-GQDs has reached up to 10.2%. High-resolution spectra of N 1s indicate the nitrogen atoms are typically in the form of pyridine-like (80% of integral area) and pyrrole-like structure. The dominating existence of pyridine nitrogen indicates that most of the nitrogen atoms are bonded with carbon in five-member ring structures and are distributed on the surface of GQDs. In accordance with the results of XPS, the spectra of FTIR and ^{13}C NMR (shown Figure 6) both demonstrate that the numerous chemical groups of $-CH_2-NH-$ or $-CNH_2$ emerge on FR-GQDs. Thus, it is reasonable to conclude that the appearance of amide groups on carbon dots (C-dots) significantly suppresses nonradiative recombination due to localized electron–hole pairs, thereby enhancing the intrinsic emission of carbon dots and eventually raising the QYs of FR-GQDs up to 77%.

3.3. Mechanism of Photostability

The excited fluorophore resided in the first singlet excited state (S_1) can further experience an intersystem crossing to a nonradiative triplet excited state (T_1).[5b] Fluorophore in the T_1 state will transfer electrons to the oxygen, water, or other biological molecules resulting in the formation of certain reactive oxygen species (ROS) such as superoxide radical ($O_2^{\bullet-}$), singlet oxygen ($^1O_2$), and hydroxyl radical ($OH^{\bullet}$). These active radical species degrade the fluorophore leading to photobleaching. In our case, FR-GQDs samples for analysis are taken at the beginning and after 360 min of the exposure procedure, and their UV–vis, FTIR, and ^{13}C NMR vibration spectra are recorded and compared to investigate the impact of ROS on FR-GQDs.

As shown in **Figure 7**a–c, all the characteristic vibration peaks match perfectly showing the excellent stability of FR-GQDs during photobleaching. In detail, UV–vis spectra exhibit no variation. FTIR and ^{13}C NMR spectra show a small decrease in the peaks intensity in which vibration at 1589 cm^{-1} can be attributed to NH_2 vibration. Furthermore, the ROS production of FR-GQDs under UV irradiation is measured and compared with that of a common photocatalytic material titanium dioxide (TiO_2 (P25), Degussa, Germany). It can be observed in Figure 7d that the ROS production of FR-GQDs is about 52–56% of the titanium dioxide which indicates that the ROS concentration is at a relatively low level during photobleaching. Previous research indicates that the three hydroxymethyl groups of tris can form a corn-like structure around the fluorescent center effectively suppressing the diffusion of oxygen and other radical species, slowing down the degradation of photobleaching.[25]

Thus, it can be concluded that inherent stability of graphene nucleus, surface molecular structure of FR-GQDs, and relatively low ROS levels collectively lead to high stability against photobleaching.

3.4. Mechanism of Cancer Targeting

Earlier breakthrough work revealed that pterin group is essential for folic acid to anchor the binding pocket of folate receptor. In other words, without the binding effect of pterin, the FR targeting ability of folic acid is lost. Recently, several works have proved that although the FA are fabricated into C-dots, the function of FR cancer targeting still exists. However, the detail targeting mechanism for these C-dots is not investigated.[26] In this study, the analyses of UV–vis, FTIR, and ^{13}C NMR of FR-GQDs in Figure 6 evidence that the pterin of folic acid (commonly considered responsible for FR binding) is destroyed. Remarkably, the cancer targeting ability of FR-GQDs through binding with FR remains functional, as can be seen in Figure 3. Furthermore, the FR-GQDs also feature intracellular trafficking mechanism and intracellular distribution that are quite similar to the folic acid. According to the previous report, the interactions between the C—N, N—C=O, and N—C—N groups of pterin and amino acid residues of FR through the hydrogen and hydrophobic bonds play a decisive role in the process of FR binding.[3a] Here, we find that (as shown in Figure 6d) during the thermal process, pterin aromatic nucleus of the folic acid is (at least partially) destroyed, while the C—N, N—C=O, and N—C—N groups still remain and are distributed on the FR-GQDs surface.

This interesting phenomenon may thus be explained as follows. The residual chemical groups of C—N, N—C=O, and N—C—N are still able to bond with the FR, leading to effective FR-GQDs internalization through the FR endocytosis mechanism. However, we emphasize that the results of our studies only unambiguously confirm the fact that the FR-GQDs are internalized through the FR expressed on the cell surface and indicate the functional groups that most likely cause the binding between the FR and GQDs. Further studies, especially at the atomic level, would shed more light on the possible effective controls of the interactions between the FR-GQDs and FR leading to the practically important selectivity in cellular responses.[3a]

4. Conclusion

In this study, graphene quantum dots named as FR-GQDs with high QYs (77%) were prepared using a simple one-step hydrothermal conversion of folic acid and tris(hydroxymethyl) aminomethane at a mild temperature (220 °C). Cell viability experiments indicate that this water-soluble GQDs exhibited good cancer targeting ability through the folate receptor binding without showing any cytotoxicity. Further characterizations evidence that the FR-GQDs are extremely photostable (90.81 $mWcm^{-2}$ for 360 min) and thermally stable (0–95 °C). In combination with these excellent properties the FR-GQDs prepared in this study are highly promising for targeting cancer diagnosis and therapy. Furthermore, the research also finds that even though pterin moiety of folic acid is destroyed, the FR targeting ability is retained, while a much better QY and stability properties are demonstrated. The mechanism behind this interesting phenomenon opens an opportunity for performance improvement of pterin derivatives in future research and applications.

5. Experimental Section

Synthesis of FR-GQDs: Folic acid (294 mg, 97%, Shanghai, China) and tris(hydroxymethyl) aminomethane (40 mg, Shanghai, China) were dissolved in 15 mL of deionized water. The mixture solution was treated with 5 min ultrasound process. The pH of obtained suspension was adjusted to neutral using sodium hydroxide (Shanghai, China) solution (0.1 mmol mL^{-1}). Then 15 mL of the transparent yellow solution was transferred into polytetrafluoroethylene autoclaves. After heating at 220 °C for 6 h, dark brown solution was obtained. By centrifuging at 6000 rpm min^{-1} for 16 min and filtrating through 22 µm ultrafiltration membrane, the sediments were removed. Then the clear brownish black solution was dialyzed against the deionized water for 6 h and freeze-dried under vacuum condition. For biological application, these productions were further dissolved in PBS solution (pH = 7).

Measurements: Morphology structure was characterized using transmission electron microscope (JEOL, JEM-2100F, Japan) and Raman spectroscopy (Jobin Yvon Lab RAM HR 800 UV micro-Raman spectrometer, France). Particle components were analyzed by XPS (AXIS ULTRA DLD, Kratos, Japan). Optical vibration spectra were characterized by fluorescence spectroscopy (F-2700 Hitachi, Japan), UV–vis absorption spectroscopy (Avaspec-2048-2-USB2, Avantes, Netherlands), and Fourier transform infrared spectrometer (Nicolet 6700, Thermo Scientific, USA). Chemical groups were analyzed using 600 MHz nuclear magnetic (Avance III 600 MHz, Germany) and FTIR (Nicolet 6700, Thermo Scientific, USA). Cells were imaged in the fluorescence microscope (Carl Zeiss, Axio Vert.A1, Germany) and confocal microscopy (Leica SP8, Germany). Cytotoxicity assay and fluorescent quantitative analyses were conducted by automatic microplate reader (Infinite 200PRO, Tecan, Switzerland).

Measurement of QYs: The QYs of the produced FR-GQDs were measured by using quinine sulfate (dissolved in 0.1 M H_2SO_4, QYs = 54%) as a reference. The QYs of the obtained FR-GQDs were calculated according to the formula

$$\Phi_{sm} = \Phi_{st}\left(\frac{Grad_{sm}}{Grad_{st}}\right)\left(\frac{\eta_{sm}^2}{\eta_{st}^2}\right) \quad (1)$$

where Φ indicates the QYs, Grad indicates the gradient of the linear plot from integrated fluorescence intensity versus absorbance, and η represents the refractive index (both 1.33) of the measuring solvent. Subscript "st" and subscript "sm" are the abbreviations of standard (quinine sulfate) and samples of FR-GQDs, respectively. UV–vis absorbance of quinine sulfate and FR-GQDs were estimated at 330 nm, kept below 0.1 in a 10 mm cuvette. The integrated intensity of FL spectra was calculated under the area of FL curve ranging from 340 to 700 nm excited under wavelength of 330 nm.

Cell Experiments: Cancer Cell Imaging: Standard Fluorescence Imaging: Cell lines (SKOV3, MDA-MB-231, MCF7, BMSC; ATCC) were triply seeded in 12-well cell culture plates cultivated for 24 h. FR-GQDs solution at a final concentration of 200 µg mL^{-1} was added to each well at pH = 7 (adjusted by PBS). Then the cells were incubated for another 4 h and subsequently washed with PBS for three times to eliminate the unabsorbed FR-GQDs completely. After fixing with formaldehyde solution and washed carefully, the cells were placed under fluorescence microscope exciting at the wavelength ranging from 330 to 400 nm (centered at 360 nm) for fluorescence image observation.

Confocal Fluorescence Imaging: Cells of SKOV3 were triply seeded in a confocal cell culture plate cultivated for 24 h. FR-GQDs solution was added to each well at pH = 7 (adjusted by PBS). Then the cells were, respectively, incubated for 1, 2, 3, 6, and 18 h and subsequently washed with PBS for three times to eliminate the unabsorbed FR-GQDs completely. After fixing with formaldehyde solution and washed carefully, the cells were placed under confocal microscope for fluorescence image observation.

Fluorescence Quantitative Analyses: Cells (5×10^3 well^{-1}) of SKOV3, MDA-MB-231, MCF7, and BMSC were triply seeded in UV–transparent 96-well (Corning3635, American) cell culture plates cultivating for 24 h. FR-GQDs samples at final concentration of 100 and 200 μg mL^{-1} were added to each well at pH = 7 and subsequently incubated for 4 h. After washing with PBS for three times, the treated cells were excited at 330 nm and the FL intensity at wavelength of 395.5 nm was recorded using an automatic microplate reader (Infinite 200PRO, Tecan, Switzerland).

Competitive Effect of Free FA on FR-GQDs Cellular Uptake: Folic acid was dissolved in $NaHCO_3$ solution (0.3 wt%) at an initial concentration of 4 mg mL^{-1}. Cells (1×10^4 well^{-1}) of SKOV3 were triply seeded in UV–transparent 96-well (Corning3635, American) cell culture plates cultivated for 24 h. Then cells were pretreated with folic acid for 12 h at final concentrations ranging from 50 to 1000 μg mL^{-1}. After washing with PBS for three times, FR-GQDs samples at final concentration of 100 μg mL^{-1} were added to each well and cultivated for 4 h. Subsequently, the cell groups were further washed with PBS for three times to remove the unabsorbed FR-GQDs in the culture medium. Finally, the FL intensity of FR-GQDs inside the cells was recorded using the automatic microplate reader.

Cytotoxicity: Cells (5×10^3 well^{-1}) (MCF7, SKOV3, MDA-MB-231, Cal-27, NH6, BMSC; ATCC) were triply cultivated in 96-well plates cultivating for 24 h. FR-GQDs samples of different final concentrations (0, 200, 400, 600, 800, and 1000 μg mL^{-1}) were added to each well and subsequently incubated for another 24 h. After washing with PBS, CCK-8 solution was added into the cell well for 4 h incubation. The absorbance was measured at 560 nm. Cell viability was determined by comparing the absorbance value with that of control cells which did not take in any FR-GQDs except equal necessary culture medium.

Supporting Information

Supporting Information is available from the Wiley Online Library or from the author.

Acknowledgements

This research was supported by the National Natural Science Foundation of China (Grant Nos. 11675109 and 31400859) and Biomedical Engineering Cross Research Foundation of Shanghai Jiao Tong University (Grant Nos. YG2016MS12 and YG2013MS60). K.O. thanks the Australian Research Council for partial support.

Conflict of Interest

The authors declare no conflict of interest.

Keywords

cancer, folate receptors, folic acid, graphene quantum dots, luminescence

Received: August 22, 2018
Revised: October 31, 2018
Published online: December 13, 2018

[1] a) J. Fridlyand, R. M. Simon, J. C. Walrath, N. Roach, R. Buller, D. P. Schenkein, K. T. Flaherty, J. D. Allen, E. V. Sigal, H. I. Scher, *Nat. Rev. Drug Discovery* **2013**, *12*, 743; b) R. R. Zhang, A. B. Schroeder, J. J. Grudzinski, E. L. Rosenthal, J. M. Warram, A. N. Pinchuk, K. W. Eliceiri, J. S. Kuo, J. P. Weichert, *Nat. Rev. Clin. Oncol.* **2017**, *14*, 347.

[2] a) M. Razzak, *Nat. Rev. Clin. Oncol.* **2013**, *10*, 668; b) C. Y. Lin, J. Gustafsson, *Nat. Rev. Cancer* **2015**, *15*, 216.

[3] a) C. Chen, J. Ke, X. E. Zhou, W. Yi, J. S. Brunzelle, J. Li, E. L. Yong, H. E. Xu, K. Melcher, *Nature* **2013**, *500*, 486; b) A. S. Wibowo, M. Singh, K. M. Reeder, J. J. Carter, A. R. Kovach, W. Meng, M. Ratnam, F. Zhang, R. C. Dann, *Proc. Natl. Acad. Sci. USA* **2013**, *110*, 15180.

[4] a) G. M. van Dam, G. Themelis, L. M. Crane, N. J. Harlaar, R. G. Pleijhuis, W. Kelder, A. Sarantopoulos, J. S. de Jong, H. J. Arts, V. D. Z. Ag, *Nat. Med.* **2011**, *17*, 1315; b) X. Gao, Y. Cui, R. M. Levenson, L. W. Chung, S. Nie, *Nat. Biotechnol.* **2004**, *22*, 969; c) P. K. Jain, I. H. El-Sayed, M. A. El-Sayed, *Nano Today* **2007**, *2*, 18.

[5] a) Q. Zheng, M. F. Juette, S. Jockusch, M. R. Wasserman, Z. Zhou, R. B. Altman, S. C. Blanchard, *Chem. Soc. Rev.* **2014**, *43*, 1044; b) A. R. Gliga, S. Sara, O. W. Inger, F. Bengt, H. L. Karlsson, *Part. Fibre Toxicol.* **2014**, *11*, 11.

[6] X. T. Zheng, A. Ananthanarayanan, K. Q. Luo, P. Chen, *Small* **2015**, *11*, 1620.

[7] B. Kong, A. Zhu, C. Ding, X. Zhao, B. Li, Y. Tian, *Adv. Mater.* **2012**, *24*, 5844.

[8] a) S. Zhu, Q. Meng, L. Wang, J. Zhang, Y. Song, H. Jin, K. Zhang, H. Sun, H. Wang, B. Yang, *Angew. Chem., Int. Ed.* **2013**, *52*, 3953; b) J. Wang, P. Zhang, C. Huang, G. Liu, K. C. Leung, Y. X. WÃ ng, *Langmuir* **2015**, *31*, 8063.

[9] N. Parker, M. J. Turk, E. Westrick, J. D. Lewis, P. S. Low, C. P. Leamon, *Anal. Biochem.* **2005**, *338*, 284.

[10] Y. G. Assaraf, C. P. Leamon, J. A. Reddy, *Drug Resist. Updates* **2014**, *17*, 89.

[11] A. M. Gazzali, M. Lobry, L. Colombeau, S. Acherar, H. Azaïs, S. Mordon, P. Arnoux, F. Baros, R. Vanderesse, C. Frochot, *Eur. J. Pharm. Sci.* **2016**, *93*, 419.

[12] a) A. V. Vorobei, P. A. Vorobei, *J. Appl. Spectrosc.* **2011**, *78*, 614; b) M. K. Off, A. E. Steindal, A. C. Porojnicu, A. Juzeniene, A. Vorobey, A. Johnsson, J. Moan, *J. Appl. Spectrosc.* **2005**, *80*, 47.

[13] a) Z. Li, H. Yu, T. Bian, Y. Zhao, C. Zhou, L. Shang, Y. Liu, L. Z. Wu, C. H. Tung, T. Zhang, *J. Mater. Chem. C* **2015**, *3*, 1922; b) G. Beamson, D. Briggs, *High Resolution XPS of Organic Polymers: The Scienta ESCA300 Database*, Wiley, New York **1992**; c) J. Russat, *Surf. Interface Anal.* **1988**, *11*, 414.

[14] a) J. Hou, W. Wang, T. Zhou, B. Wang, H. Li, L. Ding, *Nanoscale* **2016**, *8*, 11185; b) Z. H. Sheng, L. Shao, J. J. Chen, W. J. Bao, F. B. Wang, X. H. Xia, *ACS Nano* **2011**, *5*, 4350.

[15] a) N. Parvin, T. K. Mandal, *RSC Adv.* **2016**, *6*, 18134; b) D. T. Clark, W. J. Feast, P. J. Tweedale, H. R. Thomas, *J. Polym. Sci., Polym. Chem. Ed.* **1980**, *18*, 1651.

[16] a) N. F. Saba, X. Wang, S. Müller, M. Tighiouart, K. Cho, S. Nie, Z. Chen, D. M. Shin, *Head Neck* **2009**, *31*, 475; b) Y. Choi, S. Kim, M. H. Choi, S. R. Ryoo, J. Park, D. H. Min, B. S. Kim, *Adv. Funct. Mater.* **2014**, *24*, 5781.

[17] D. J. Bharali, D. W. Lucey, H. Jayakumar, H. E. P. And, P. N. Prasad, *J. Am. Chem. Soc.* **2005**, *127*, 11364.

[18] A. H. Thomas, C. Lorente, A. L. Capparelli, M. R. Pokhrel, A. M. Braun, E. Oliveros, *Photochem. Photobiol. Sci.* **2002**, *1*, 421.

[19] J. Zhang, S. Rana, R. S. Srivastava, R. D. Misra, *Acta Biomater.* **2008**, *4*, 40.

[20] Y. Y. He, X. C. Wang, P. K. Jin, B. Zhao, X. Fan, *Spectrochim. Acta, Part A* **2009**, *72*, 876.

[21] a) M. Murata, H. Tanaka, S. Omura, *J. Antibiot.* **1987**, *40*, 251; b) http://chemdb.sgst.cn/ssdb/main/NMR_introduce.asp, Shanghai

Institute of Organic Chemistry, Chinese Academy of Sciences, **2018**.
[22] S. J. Zhu, Y. B. Song, X. H. Zhao, J. R. Shao, J. H. Zhang, B. Yang, *Nano Res.* **2015**, *8*, 355.
[23] a) S. Zhu, J. Zhang, S. Tang, C. Qiao, L. Wang, H. Wang, X. Liu, B. Li, Y. Li, W. Yu, *Adv. Funct. Mater.* **2012**, *22*, 4732; b) L. Lin, M. Rong, S. Lu, X. Song, Y. Zhong, J. Yan, Y. Wang, X. Chen, *Nanoscale* **2015**, *7*, 1872.
[24] a) Y. Q. Zhang, X. Y. Liu, Y. Fan, X. Y. Guo, L. Zhou, Y. Lv, J. Lin, *Nanoscale* **2016**, *8*, 15281; b) D. Qu, M. Zheng, L. G. Zhang, H. F. Zhao, Z. G. Xie, X. B. Jing, R. E. Haddad, H. Y. Fan, Z. C. Sun, *Sci. Rep.* **2014**, *4*, 5294.
[25] Y. Liu, L. Zhou, Y. Li, R. Deng, H. Zhang, *Nanoscale* **2017**, *9*, 491.
[26] a) S. Bhunia, A. Maity, S. Nandi, D. Stepensky, R. Jelinek, *ChemBioChem* **2016**, *17*, 614; b) H. Liu, Z. Li, Y. Sun, X. Geng, Y. Hu, H. Meng, J. Ge, L. Qu, *Sci. Rep.* **2018**, *8*, 1086.